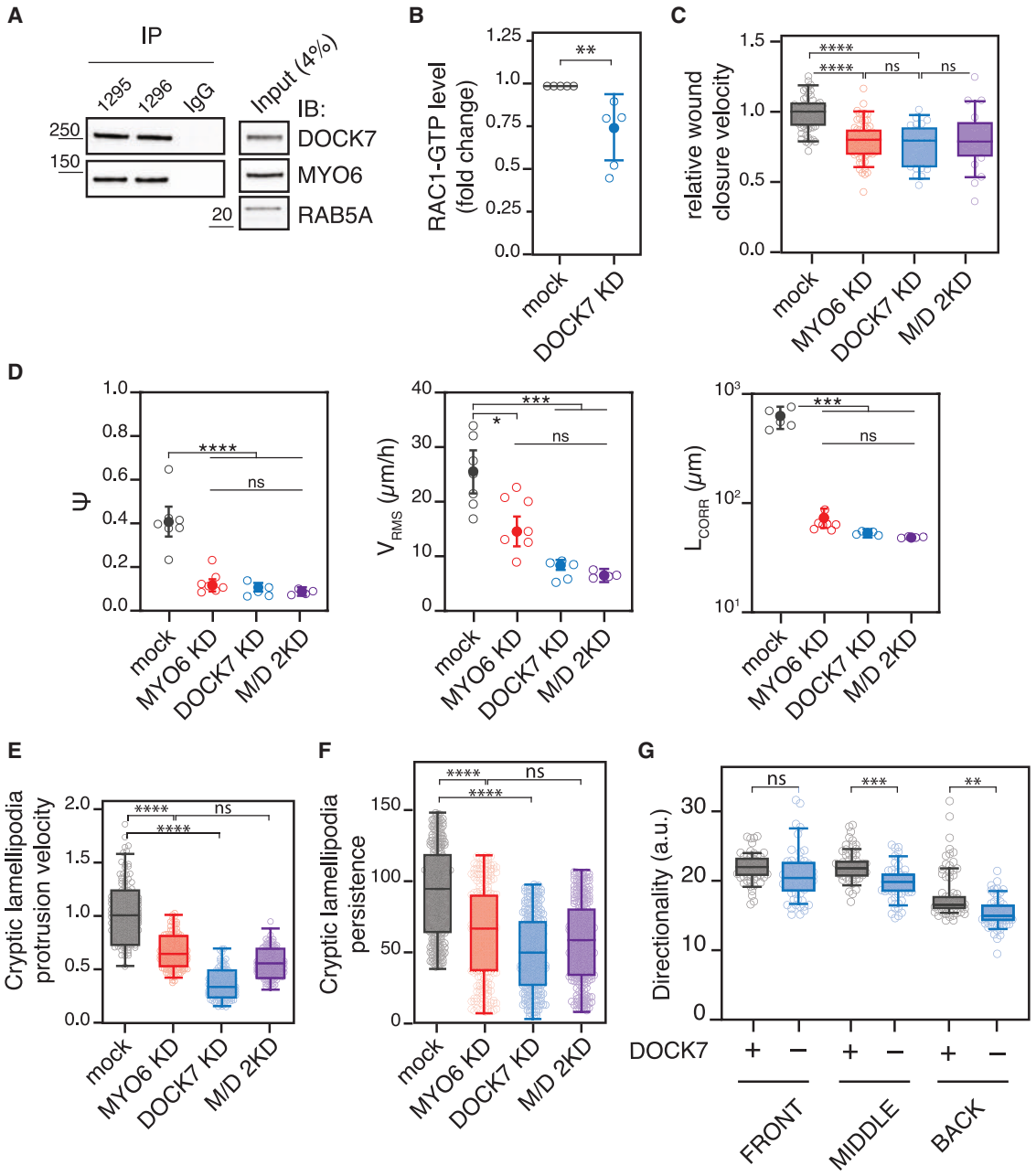

Figure 4. A MYO6-DOCK7 axis activates RAC1 in a planar polarized fashion

(A) Immunoprecipitation (IP) analysis of DCIS-RAB5A cells with two antibodies against myosin VI (1295 and 1296) and rabbit immunoglobulin G (IgG) as a negative control. IB as indicated.

(B) GST-CRIB assay quantification from mock or DOCK7 KD monolayers. Data are reported as fold change with respect to RAC1-GTP level in the corresponding mock sample for each experiment. n = 5 independent experiments. Reported values are mean ± SD. **p < 0.01 by Student's t test.

(C) Wound healing assay results for mock, MYO6 KD, DOCK7 KD, and the combination of MYO6- and DOCK7-depleted (M/D 2KD) cells. The average wound closure speed relative to the mock condition is plotted in the graph. The empty circle represents the mean wound closure velocity quantified for each video. n ≥ 15 (3 independent experiments). ns > 0.999, ****p < 0.0001 by ANOVA.

(D) PIV analysis of the streaming of the indicated cell monolayers. From left to right: orientational order parameter ψ, root-mean-squared velocity V_{RMS}, and correlation length L_{CORR}. The corresponding average stretching exponent β is 0.68 ± 0.1, 0.74 ± 0.06, 0.84 ± 0.07, and 0.87 ± 0.1 for mock, MYO6 KD, DOCK7 KD, and M/D 2KD, respectively. Empty circle, mean of each experiment calculated from five videos/condition (six independent experiments). Error bars ±SD. ns > 0.999, *p < 0.05, ***p < 0.001, ****p < 0.0001 by ANOVA.

(E) Quantification of cryptic lamellipodium protrusion velocity performed as in Figure 2D for the indicated cell lines. n = 158 (4 independent experiments).

(legend continued on next page)

interactome, which we identified in a previous study.[25] Among the myosin VI interactors, we focused on the human dedicator of cytokinesis DOCK7,[31,44,45] a dual guanine nucleotide exchange factor (GEF) for RAC1 and CDC42 GTPase.[46] We first confirmed that myosin VI and DOCK7 co-immunoprecipitated in DCIS-RAB5A cells (Figure 4A). Next, we tested the functional involvement of DOCK7 in regulation of RAC1 activity in cryptic lamellipodia in our model of flocking fluid motility in monolayers.

Biochemically, DOCK7 depletion significantly reduced RAC1-GTP levels (Figure 4B). Functionally, DOCK7 KD cells showed impaired collective migration in wound healing (Figure 4C; Video S9) and streaming assays (Figure 4D Video S10) to the same extent as in myosin VI KD cells. Intriguingly, concomitant silencing of DOCK7 and myosin VI did not worsen the migratory defects, suggesting that DOCK7 is likely the main effector of myosin VI activity in this context (Figures 4C and 4D). The results were confirmed by a second siRNA DOCK7 oligo (Figures S4A and S4B).

Next, we tested whether DOCK7-dependent impairment of flocking monolayer migration was due to a lack of oriented and persistent cryptic lamellipodia. By exploiting EGFP-LifeAct mosaic cells in confluent monolayers, we discovered that protrusion velocity and persistence of cryptic lamellipodia are similarly impaired after individual or concomitant depletion of DOCK7 and myosin VI (M/D 2KD) (Figures 4E and 4F). We then used cell segmentation and tracking of H2B-mCherry-labeled monolayer cells in a wound healing assay to specifically analyze migration of the leader or follower cells. Consistent with data obtained in myosin VI KD cells (Figures 2G–2I), silencing of DOCK7 did not affect the lamellipodium dynamics of the cell leading edge at the wound front (Figures S4C and S4D), while kymograph-based quantification of follower cells showed a significant reduction in directionality (Figure 4G).

Prompted by these results, we reasoned that myosin VI may be required to localize DOCK7 and spatially restrict its activity toward RAC1. To test this hypothesis, we first examined DOCK7 localization in our cell system. To overcome the lack of reliable antibodies, we generated a population of EGFP-DOCK7 cells that expressed low physiological levels of the protein (Figure S4E). A confocal analysis demonstrated that, in a confluent monolayer, DOCK7 co-localized with myosin VI at apical cell-cell junctions (Figure 5A) and accumulated in cryptic lamellipodia extending basally onto the cell substrate (Figures 5B and 5C). This localization requires myosin VI because, upon myosin VI depletion, DOCK7 became diffusely distributed throughout the cytoplasm (Figure 5D) and was no longer enriched at actin-rich protrusion tips (Figures 5E and 5F).

Collectively, these data indicate that a myosin VI-DOCK7-RAC1 axis controls cryptic lamellipodium protrusions, which, in turn, are required for collective flocking locomotion.

Myosin VI directly interacts with the DOCK7 DHR2 domain

A functional interaction between myosin VI and DOCK7 has been reported previously in the neuronal context[47] as well as in HeLa[44] and HEK293T cells,[31] but the molecular basis of this interaction has not been fully explored. Structurally, both proteins are composed of several distinct domains we investigated to map the critical surface of interaction (Figure S5A). First, we confirmed that the myosin VI binding surface resides in the DHR2 domain of DOCK7[45] because removal of this GEF catalytic domain in the context of the full-length protein was sufficient to abrogate binding to the myosin VI tail (Figure 6A). To identify the minimal binding region within myosin VI, we performed a pull-down experiment with different myosin VI tail constructs. The cargo-binding domain (CBD,[44]) and the MYO6 ubiquitin-binding (MyUb[48]) isolated domains bound DOCK7, although with reduced efficiency compared with the MyUb-CBD tail of myosin VI (Figure S5B). Importantly, using bacterially expressed and purified fragments, we showed that the interaction between the DHR2 domain and the MyUb-CBD domain is direct (Figure 6B).

The DOCK family consists of 11 structurally conserved proteins that serve as atypical RHO GEFs and are differentially expressed in tissues.[49,50] We tested the ability of the MyUb-CBD tail to bind the DHR2 domain of a few prototypes of the family, including DOCK2, DOCK6, and DOCK9.[51] Surprisingly, binding was detected only for the DHR2 domain of DOCK7 (Figure 6C).

This result prompted us to further analyze the interaction surface. Despite low sequence homology among the DOCK family members, the DHR2 domains are well conserved and adopt a similar fold that is characterized by three lobes, A–C. Of them, lobes B and C are endowed with GTPase binding and GEF activity, whereas lobe A seems to be involved in homodimerization, at least in a few DOCK proteins.[49,51] By using DHR2 protein fragments, we showed that lobe A is indeed required for DOCK7 dimerization but is also critical for myosin VI interaction (Figure S5B). Lobe A is not present in the recombinant DHR2 constructs used to generate the structural data for DOCK7 (PDB: 6AJ4). Therefore, we used AlphaFold2-Multimer[52,53] to predict the DOCK7 DHR2 structure and possible myosin VI interaction surfaces. The DOCK7 DHR2 and myosin VI MyUb and CBD domains were predicted with high confidence scores, except for a linker sequence between the two myosin VI domains that most likely is flexible (Figure 6D, top panel). The best model prediction indicated that the DOCK7 lobe A domain is in contact with the CBD and MyUb domains of myosin VI, with the MyUb and CBD domains also interacting with each other (Figure 6E). This model showed high confidence for the residue-to-residue distance (Figure 6D, bottom panel) and is fully consistent with the finding that loss of either MyUb or CBD weakens the interaction with DOCK7 (Figure S5B).

A hypothesis motivated by our structure-function analysis is that the binding of myosin VI to lobe A may influence the GEF activity of DOCK7. Indeed, DOCK7 showed poor activity on RAC1 compared with DOCK2 (Figure S5C), as reported previously,[46] strongly suggesting a possible allosteric missing partner. We

(F) Quantification of cryptic lamellipodium protrusion persistence performed as in Figure 2E for the indicated cell lines. n = 250 (4 independent experiments). ns > 0.999, ****p < 0.0001 by ANOVA.

(G) Quantification of the directionality of the cells belonging to the different areas performed as in Figure 2J for the indicated cell lines. n ≥ 34 (3 independent experiments). Error bars, ±SEM. ns > 0.999, ****p < 0.0001 by ANOVA.

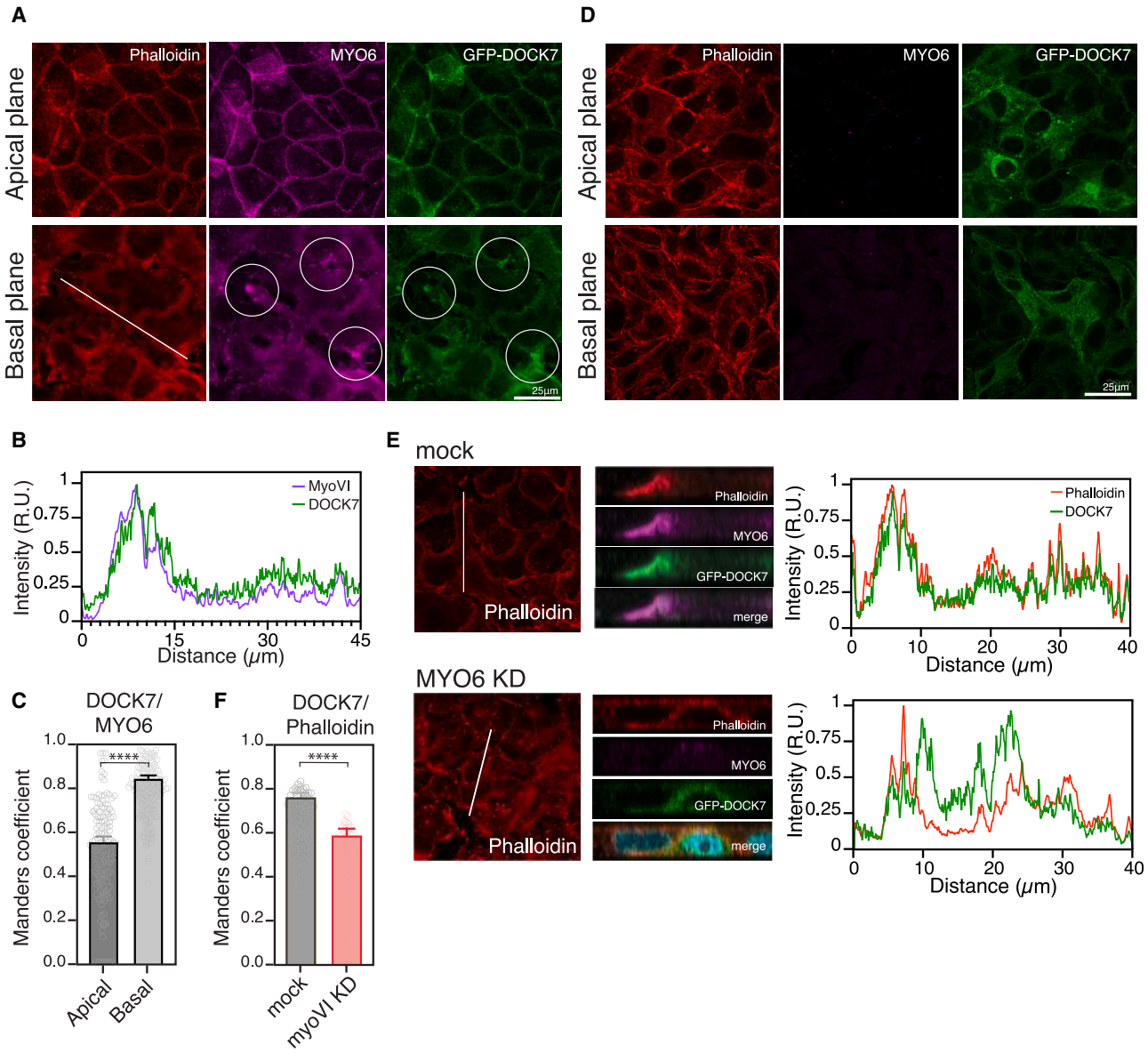

Figure 5. Myosin VI promotes local RAC1 activation by recruiting DOCK7 to cryptic lamellipodia

(A) IF analysis of GFP-DOCK7 expressing DCIS-RAB5A cells seeded in the jammed condition to visualize lamellipodium-like structures. Purple, myosin VI; red, phalloidin. Middle and basal planes are shown. Scale bars, 25 μm.

(B) Fluorescence intensity profiles show GFP-DOCK7 and MYO6 fluorescence distribution across the white line shown in (A) (x axis). The fluorescence intensities are reported on the y axis.

(C) Quantification of the colocalization of GFP-DOCK7 and myosin VI shown in (A), using Manders' coefficient. n = 153 (4 independent experiments). Error bars, ±SEM. ****p < 0.0001 by Student's t test.

(D) IF analysis of GFP-DOCK7 expressing DCIS-RAB5A cells depleted of myosin VI and seeded in the jammed condition as in (A). Purple, myosin VI; red, phalloidin. Middle and basal planes are shown.

(E) Z stacks acquisition of the cell lines described in (A) and (D). Right: fluorescence intensity profiles showing the distribution of GFP-DOCK 7 and phalloidin fluorescence across the white line (x axis).

(F) Quantification of the colocalization of GFP-DOCK7 and phalloidin in XZ images shown in (E), using Manders' coefficient. n ≥ 74 (four independent experiments). Error bars, ±SEM. ****p < 0.0001 by Student's t test.

then used a suboptimal concentration of DOCK7 and titrated in increasing amounts of the MyUb-CBD tail (Figure 6F), analyzing activity by the GEF assay. Even under these conditions, however, we failed to detect any effect of the MyUb-CBD fragment on the GEF activity of DOCK. Thus, we conclude that, while critical for DOCK7 localization, myosin VI does not appear to influence DOCK7 GEF activity toward RAC1, at least in this simplified *in vitro* experiment.

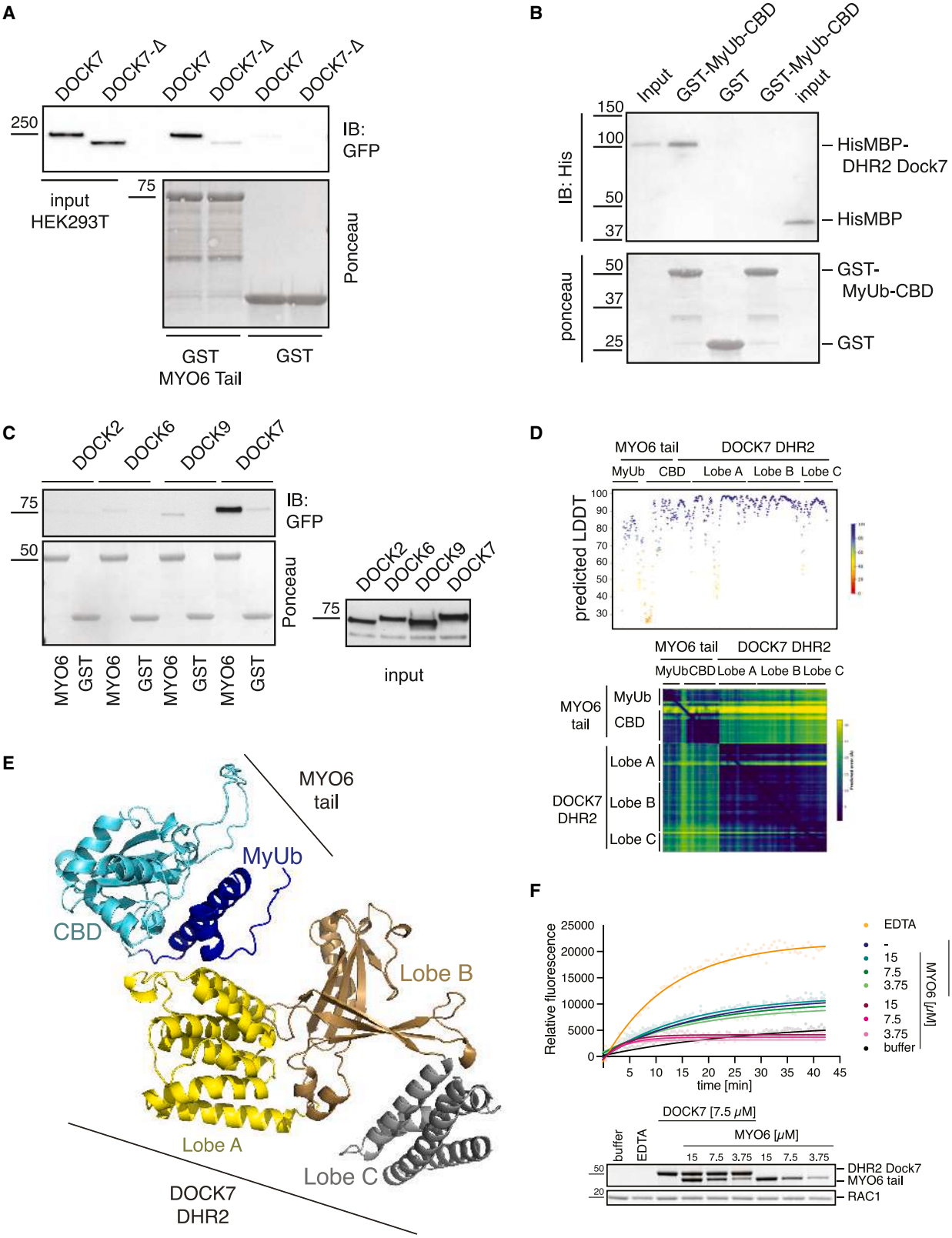

(legend on next page)

Myosin VI overexpression is exploited by infiltrating breast cancer cells

To assess the clinical relevance of our findings, we investigated the expression profile of myosin VI in human breast cancer by analyzing RNA sequencing (RNA-seq) data of The Cancer Genome Atlas (TCGA) breast tumors dataset (breast cancer [BRCA]). We assessed a total of 981 samples with complete clinical and pathological information, including molecular subtyping,[54] and we focused our attention on the myosin VI short isoform because we have demonstrated previously that this isoform is selectively required for cancer cell migration and for DOCK7 binding.[31] As shown in Figure 7A, expression of the myosin VI short isoform is significantly higher in the basal-like subtype compared with all other cancer subtypes and normal breast tissue. Notably, this subtype comprises 15%–20% of all breast tumors and largely correspond to triple-negative (TN) highly metastatic breast cancer, to which the MCF10.DCIS.com cell line belongs.

To confirm this result at the protein level, we analyzed a panel of human DCIS and invasive ductal carcinoma (IDC) tissue sections by immunohistochemistry. While diffuse and weak expression of myosin VI characterized most DCIS samples, the staining intensity was significantly higher in IDC, particularly in the infiltrating components (Figure 7B), as quantified by software analysis on digital slide scans (Figure 7C). Thus, breast carcinoma selectively increases myosin VI expression during progression from DCIS to IDC.

DISCUSSION

During carcinoma dissemination, cellular rearrangements are fostered by a solid-to-liquid transition, known as unjamming, through partially identified molecular mechanisms. We found here that myosin VI is essential to support this tissue-level phase transition because its depletion severely reduces cell coordination and impairs cell migration persistence and directionality. Molecularly, we identified DOCK7, a GEF for RAC1, as the critical and direct myosin VI interactor. Myosin VI is essential to restrict DOCK7 at cryptic lamellipodia to locally activate RAC1 and promote coordinated movement of the follower cells. This regulation may likely aid the follower cells to chase and coordinate their motion with the leaders, as recently suggested by several studies,[55,56] thereby enabling maintenance of monolayer compactness during collective motion. Our results also highlight the role exerted by RAC1 in the follower cells and show that these cells are not simply hitchhikers or passive passengers but, rather, actively contribute to promoting collective cell migration.

Our study has striking similarities with recent discoveries obtained in *Drosophila* by Campanale et al.,[55] who uncovered the role of a Scrib/Cdep/Rac pathway as essential for follower cell movement and cluster cohesion in border cell migration. In this study and context, Cdep was identified as the Rac GEF, whereas Scrib, Dlg, and Lgl aid in localizing Cdep basolaterally to activate Rac in followers. Intriguingly, *Drosophila* was the system first employed to demonstrate the critical role of myosin VI in collective motion because its depletion severely affects border cell migration.[27] Whether myosin VI does so by perturbing RAC1 activity in follower cells in conjunction with or alternatively to Scrib and Cdep has not been addressed. Likely, more than a RacGEF is required in follower cells, and little is known about the DOCK7 ortholog in *Drosophila*, Zir. Thus, it will be exciting to re-evaluate the role of myosin VI and Zir activity in border cell dynamics in light of our current finding.

It must be noted that border cells display not only a leader-to-follower topological organization but also an apicobasal polarity during their motion, consistent with their prototypical epithelial nature. Conversely, breast carcinoma MCF10.DCIS.com cells nearly completely lose their apico-basal polarity while they retain a number of features of normal epithelial tissues, including a planar polarized organization. Because the molecular determinants of these polarity programs are distinct, it is conceivable that myosin VI might be more critical when a planar polarity arrangement is needed and established but dispensable during apico-basal organization. This specific role is particularly attractive considering the selective role exerted by the alternatively spliced myosin VI isoforms.[25,31] Indeed, fully polarized epithelia selectively express myosin VI long, which is impaired in DOCK7 binding[31] and is critical for clathrin-mediated endocytosis at the apical surface.[57]

Limitations of the study

Our findings imply that the myosin VI short isoform is relevant for infiltrating carcinoma cells to ensure and enhance coordinated and directed collective invasion during unjamming. Although several lines of evidence support this idea, investigation of myosin VI isoforms has been limited to mRNA expression analysis because of the unavailability of isoform-specific antibodies for protein detection. Therefore, further investigations are needed to determine the spatial and temporal expression of the short isoform protein in different tumor subtypes. Moreover,

Figure 6. Myosin VI specifically and directly interacts with the lobe A of the DHR2 domain of DOCK7

(A) GST pull-down assay using the myosin VI tail and lysates from HEK293T cells transfected with full-length GFP-DOCK7 or its DHR2 deleted mutant, GFP-DOCK7ΔDHR2 (DOCK7Δ). IB as indicated. Ponceau shows equal loading.

(B) Pull-down assay using the HisMBP-DHR2 domain of DOCK7 and MyUb-CBD construct of myosin VI produced and purified from bacteria. IB as indicated. Ponceau shows equal loading.

(C) GST pull-down assay using MyUb-CBD of myosin VI (spanning amino acids 1,080–1,295) and lysate from HEK293T cells transfected with the GFP-DHR2 domain of the indicated DOCK proteins. IB as indicated. Ponceau shows equal loading.

(D) Confidence scores per residue generated by AlphaFold2-Multimer for the predicted fold of domains (top) and the residue-to-residue distance (bottom). LDDT, local distance difference test.

(E) Ribbon diagram of the top-scoring AlphaFold2-Multimer model of the MYO6:DOCK7 interaction obtained by entering protein sequences for the myosin VI tail, spanning residues G1048–K1262, and DOCK7 residues of the DHR2 domain spanning P775–P1196.

(F) Representative RAC1 GEF activity assay using 7.5 μM of the DHR2 domain of DOCK7 and the indicated concentration of the MyUb-CBD myosin VI. Bottom: Coomassie gel of the samples used.

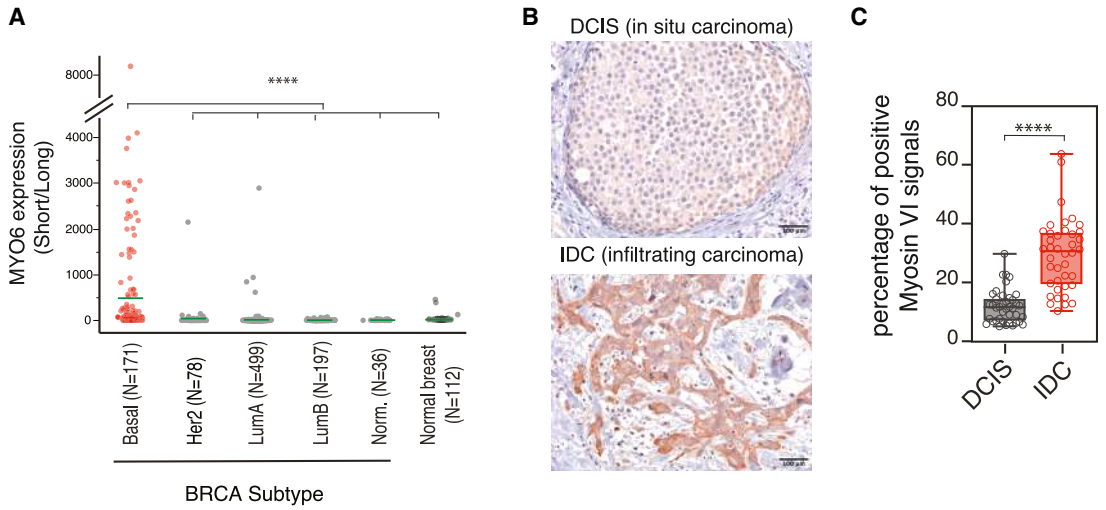

Figure 7. MYO6 is significantly overexpressed in highly metastatic breast cancers

(A) MYO6 short versus long isoform expression expressed as ratio of RPKM (reads per kilobase per million mapped reads) for the indicated BRCA subtypes. Average expression level is shown by green lines. The myosin VI short isoform was significantly overexpressed in the BRCA basal-like subtype compared with all other subtypes and normal breast tissues. Statistical significance was analyzed by one-way (chi-square approximation) Wilcoxon test. ***$p < 0.0001$.

(B) Representative immunohistochemistry (IHC) images of myosin VI in DCIS and IDC tumor sections. Original magnification, ×200. Scale bar, 100 μm.

(C) Quantitative analyses of myosin VI IHC images shown in (B). n = 40 (5 images of 8 cases/cancer type). ****$p < 0.0001$ by Student's t test.

while our results indicate that the alteration of alternative splicing mechanism of myosin VI is selected during cancer progression, the underlying process still requires clarification.

While we discovered the MYO6-DOCK7-RAC1 axis in the MCF10.DCIS.com cell line, which is representative of basal-like breast cancers, its applicability in different cellular contexts as well as murine models of breast cancer requires further investigation. To gain a comprehensive understanding of the system and establish the therapeutic potential of this critical molecular axis, further *in vitro* and *in vivo* studies are necessary. Notably, while direct inhibition of myosin VI may have unwanted deleterious effects in normal tissues,[58] the interaction surface with DOCK7 represents a promising possibility to explore in future drug discovery studies, particularly in the case of the more aggressive basal-like breast cancers for which we have limited therapeutic options.

STAR★METHODS

Detailed methods are provided in the online version of this paper and include the following:

- KEY RESOURCES TABLE
- RESOURCE AVAILABILITY
  - Lead contact
  - Materials availability
  - Data and code availability
- METHOD DETAILS
  - Constructs and reagents
  - Cell lines and transfection procedures
  - Antibodies
  - Single cell migration assay
  - Wound healing assays
  - Measurement of the cellular velocities and trajectories
  - Kymograph analysis of cell protrusions at the wound edge
  - Cell sheet streaming and kinetic parameter measurements
  - Measurements of cryptic lamellipodia dynamics
  - Immunofluorescence (IF)
  - FRET based RAC1/CDC42 activation assay
  - Protein expression and purification
  - Co-immunoprecipitation and pull-down assays
  - AlphaFold2-multimer prediction
  - GEF activity assay
  - IHC analysis and quantification
  - Expression profile analysis
- QUANTIFICATION AND STATISTICAL ANALYSIS

SUPPLEMENTAL INFORMATION

Supplemental information can be found online at https://doi.org/10.1016/j.celrep.2023.113001.

ACKNOWLEDGMENTS

We are grateful to all members of the IFOM imaging facility, in particular Francesca Casagrande, Serena Magni, and Zeno Lavagnino for support with image acquisition and analysis and Maria Grazia Totaro for support with cell sorting. This work was supported by the Associazione Italiana per Ricerca sul Cancro (investigator grant 2017-19875 to S.P., 2019-18621 and 5Xmille 22759 to G.S., and My First AIRC grant 2018-22083 to F.G.); the Seal of Excellence (SoE SEED2020 to S.P. and F.G.); the Intramural Research Program through the Center for Cancer Research, National Cancer Institute, National Institutes of Health (ZIA BC011627 to K.J.W.); and the European Union (ERC, ShapinCell-Fate, 101071470 to G.S.). The views and opinions expressed are, however, those of the author(s) only and do not necessarily reflect those of the European Union or the European Research Council Executive Agency. Neither the

European Union nor the granting authority can be held responsible for them. AlphaFold2-Multimer was run using computational resources of the High-Performance Computing Biowulf cluster of the NIH (http://hpc.nih.gov). L.M.'s work was supported by a fellowship of the Associazione Italiana per Ricerca sul Cancro. The graphical abstract was generated with BioRender.

AUTHOR CONTRIBUTIONS

Conceptualization, L.M., G.S., and S.P.; investigation, L.M. and J.W.; methodology, L.M., J.W., S.V., E. Maspero, C.A.N., V.C., A. Poli, P.M., A. Palanidessi., E.F., F.B., C.T., and K.J.W.; formal analysis, L.M., J.W., S.V., E. Martini, F.B., and K.J.W.; supervision, F.G., G.S., and S.P; data curation, L.M. and S.P.; writing – original draft, L.M. and S.P.; writing – review & editing, G.S. and S.P.; funding acquisition, S.P.

DECLARATION OF INTERESTS

The authors declare no competing interests.

INCLUSION AND DIVERSITY

We support inclusive, diverse, and equitable conduct of research.

Received: March 17, 2023
Revised: April 24, 2023
Accepted: August 1, 2023
Published: August 16, 2023

REFERENCES

1. Scarpa, E., and Mayor, R. (2016). Collective cell migration in development. J. Cell Biol. *212*, 143–155. https://doi.org/10.1083/jcb.201508047.
2. Haeger, A., Wolf, K., Zegers, M.M., and Friedl, P. (2015). Collective cell migration: guidance principles and hierarchies. Trends Cell Biol. *25*, 556–566. https://doi.org/10.1016/j.tcb.2015.06.003.
3. Friedl, P., and Wolf, K. (2010). Plasticity of cell migration: a multiscale tuning model. J. Cell Biol. *188*, 11–19. https://doi.org/10.1083/jcb.200909003.
4. Friedl, P., and Gilmour, D. (2009). Collective cell migration in morphogenesis, regeneration and cancer. Nat. Rev. Mol. Cell Biol. *10*, 445–457. https://doi.org/10.1038/nrm2720.
5. Barriga, E.H., Franze, K., Charras, G., and Mayor, R. (2018). Tissue stiffening coordinates morphogenesis by triggering collective cell migration in vivo. Nature *554*, 523–527. https://doi.org/10.1038/nature25742.
6. Qin, L., Yang, D., Yi, W., Cao, H., and Xiao, G. (2021). Roles of leader and follower cells in collective cell migration. Mol. Biol. Cell *32*, 1267–1272. https://doi.org/10.1091/mbc.E20-10-0681.
7. Szabó, B., Szöllösi, G.J., Gönci, B., Jurányi, Z., Selmeczi, D., and Vicsek, T. (2006). Phase transition in the collective migration of tissue cells: Experiment and model. Phys. Rev. *74*, 061908. https://doi.org/10.1103/PhysRevE.74.061908.
8. Angelini, T.E., Hannezo, E., Trepat, X., Marquez, M., Fredberg, J.J., and Weitz, D.A. (2011). Glass-like dynamics of collective cell migration. Proc. Natl. Acad. Sci. USA *108*, 4714–4719. https://doi.org/10.1073/pnas.1010059108.
9. Giavazzi, F., Paoluzzi, M., Macchi, M., Bi, D., Scita, G., Manning, M.L., Cerbino, R., and Marchetti, M.C. (2018). Flocking transitions in confluent tissues. Soft Matter *14*, 3471–3477. https://doi.org/10.1039/C8SM00126J.
10. Hakim, V., and Silberzan, P. (2017). Collective cell migration: a physics perspective. Rep. Prog. Phys. *80*, 076601. https://doi.org/10.1088/1361-6633/aa65ef.
11. Krause, M., and Gautreau, A. (2014). Steering cell migration: lamellipodium dynamics and the regulation of directional persistence. Nat. Rev. Mol. Cell Biol. *15*, 577–590. https://doi.org/10.1038/nrm3861.
12. Farooqui, R., and Fenteany, G. (2005). Multiple rows of cells behind an epithelial wound edge extend cryptic lamellipodia to collectively drive cell-sheet movement. J. Cell Sci. *118*, 51–63. https://doi.org/10.1242/jcs.01577.
13. Barlan, K., Cetera, M., and Horne-Badovinac, S. (2017). Fat2 and Lar Define a Basally Localized Planar Signaling System Controlling Collective Cell Migration. Dev. Cell *40*, 467–477.e5. https://doi.org/10.1016/j.devcel.2017.02.003.
14. Malinverno, C., Corallino, S., Giavazzi, F., Bergert, M., Li, Q., Leoni, M., Disanza, A., Frittoli, E., Oldani, A., Martini, E., et al. (2017). Endocytic reawakening of motility in jammed epithelia. Nat. Mater. *16*, 587–596. https://doi.org/10.1038/nmat4848.
15. Park, J.-A., Atia, L., Mitchel, J.A., Fredberg, J.J., and Butler, J.P. (2016). Collective migration and cell jamming in asthma, cancer and development. J. Cell Sci. *129*, 3375–3383. https://doi.org/10.1242/jcs.187922.
16. Frittoli, E., Palamidessi, A., Marighetti, P., Confalonieri, S., Bianchi, F., Malinverno, C., Mazzarol, G., Viale, G., Martin-Padura, I., Garré, M., et al. (2014). A RAB5/RAB4 recycling circuitry induces a proteolytic invasive program and promotes tumor dissemination. J. Cell Biol. *206*, 307–328. https://doi.org/10.1083/jcb.201403127.
17. Palamidessi, A., Malinverno, C., Frittoli, E., Corallino, S., Barbieri, E., Sigismund, S., Beznoussenko, G.V., Martini, E., Garre, M., Ferrara, I., et al. (2019). Unjamming overcomes kinetic and proliferation arrest in terminally differentiated cells and promotes collective motility of carcinoma. Nat. Mater. *18*, 1252–1263. https://doi.org/10.1038/s41563-019-0425-1.
18. Giavazzi, F., Malinverno, C., Corallino, S., Ginelli, F., Scita, G., and Cerbino, R. (2017). Giant fluctuations and structural effects in a flocking epithelium. J. Phys. D Appl. Phys. *50*, 384003. https://doi.org/10.1088/1361-6463/aa7f8e.
19. Ridley, A.J. (2015). Rho GTPase signalling in cell migration. Curr. Opin. Cell Biol. *36*, 103–112. https://doi.org/10.1016/j.ceb.2015.08.005.
20. Xi, W., Sonam, S., Beng Saw, T., Ladoux, B., and Teck Lim, C. (2017). Emergent patterns of collective cell migration under tubular confinement. Nat. Commun. *8*, 1517. https://doi.org/10.1038/s41467-017-01390-x.
21. Omelchenko, T., Vasiliev, J.M., Gelfand, I.M., Feder, H.H., and Bonder, E.M. (2003). Rho-dependent formation of epithelial "leader" cells during wound healing. Proc. Natl. Acad. Sci. USA *100*, 10788–10793. https://doi.org/10.1073/pnas.1834401100.
22. Gov, N.S. (2007). Collective cell migration patterns: Follow the leader. Proc. Natl. Acad. Sci. USA *104*, 15970–15971. https://doi.org/10.1073/pnas.0708037104.
23. Poujade, M., Grasland-Mongrain, E., Hertzog, A., Jouanneau, J., Chavrier, P., Ladoux, B., Buguin, A., and Silberzan, P. (2007). Collective migration of an epithelial monolayer in response to a model wound. Proc. Natl. Acad. Sci. USA *104*, 15988–15993. https://doi.org/10.1073/pnas.0705062104.
24. Sweeney, H.L., and Houdusse, A. (2007). What can myosin VI do in cells? Curr. Opin. Cell Biol. *19*, 57–66. https://doi.org/10.1016/j.ceb.2006.12.005.
25. Magistrati, E., and Polo, S. (2021). Myomics: myosin VI structural and functional plasticity. Curr. Opin. Struct. Biol. *67*, 33–40. https://doi.org/10.1016/j.sbi.2020.09.005.
26. Chibalina, M.V., Puri, C., Kendrick-Jones, J., and Buss, F. (2009). Potential roles of myosin VI in cell motility. Biochem. Soc. Trans. *37*, 966–970. https://doi.org/10.1042/BST0370966.
27. Geisbrecht, E.R., and Montell, D.J. (2002). Myosin VI is required for E-cadherin-mediated border cell migration. Nat. Cell Biol. *4*, 616–620. https://doi.org/10.1038/ncb830.
28. Yoshida, H., Cheng, W., Hung, J., Montell, D., Geisbrecht, E., Rosen, D., Liu, J., and Naora, H. (2004). Lessons from border cell migration in the Drosophila ovary: A role for myosin VI in dissemination of human ovarian cancer. Proc. Natl. Acad. Sci. USA *101*, 8144–8149. https://doi.org/10.1073/pnas.0400400101.

29. Dunn, T.A., Chen, S., Faith, D.A., Hicks, J.L., Platz, E.A., Chen, Y., Ewing, C.M., Sauvageot, J., Isaacs, W.B., De Marzo, A.M., and Luo, J. (2006). A novel role of myosin VI in human prostate cancer. Am. J. Pathol. *169*, 1843–1854. https://doi.org/10.2353/ajpath.2006.060316.

30. Wang, H., Wang, B., Zhu, W., and Yang, Z. (2015). Retracted: Lentivirus-Mediated Knockdown of Myosin VI Inhibits Cell Proliferation of Breast Cancer Cell. Cancer Biother. Radiopharm. *30*, 330–335. https://doi.org/10.1089/cbr.2014.1759.

31. Wollscheid, H.-P., Biancospino, M., He, F., Magistrati, E., Molteni, E., Lupia, M., Soffientini, P., Rottner, K., Cavallaro, U., Pozzoli, U., et al. (2016). Diverse functions of myosin VI elucidated by an isoform-specific α-helix domain. Nat. Struct. Mol. Biol. *23*, 300–308. https://doi.org/10.1038/nsmb.3187.

32. Acharya, B.R., Nestor-Bergmann, A., Liang, X., Gupta, S., Duszyc, K., Gauquelin, E., Gomez, G.A., Budnar, S., Marcq, P., Jensen, O.E., et al. (2018). A Mechanosensitive RhoA Pathway that Protects Epithelia against Acute Tensile Stress. Dev. Cell *47*, 439–452.e6. https://doi.org/10.1016/j.devcel.2018.09.016.

33. Maddugoda, M.P., Crampton, M.S., Shewan, A.M., and Yap, A.S. (2007). Myosin VI and vinculin cooperate during the morphogenesis of cadherin cell–cell contacts in mammalian epithelial cells. J. Cell Biol. *178*, 529–540. https://doi.org/10.1083/jcb.200612042.

34. Mangold, S., Norwood, S.J., Yap, A.S., and Collins, B.M. (2012). The juxtamembrane domain of the E-cadherin cytoplasmic tail contributes to its interaction with Myosin VI. BioArchitecture *2*, 185–188. https://doi.org/10.4161/bioa.22082.

35. Ozawa, M., Hiver, S., Yamamoto, T., Shibata, T., Upadhyayula, S., Mimori-Kiyosue, Y., and Takeichi, M. (2020). Adherens junction regulates cryptic lamellipodia formation for epithelial cell migration. J. Cell Biol. *219*, e202006196. https://doi.org/10.1083/jcb.202006196.

36. Grützmacher, S., Kemkemer, R., Thies, C., and Curio, C. (2018). Detecting Lamellipodia in Epithelial Cell Clusters Using a Fully Convolutional Neural Network for Phase Contrast. Microscopy Images *4*, 449–452. https://doi.org/10.1515/cdbme-2018-0107.

37. Fritz, R.D., Menshykau, D., Martin, K., Reimann, A., Pontelli, V., and Pertz, O. (2015). SrGAP2-Dependent Integration of Membrane Geometry and Slit-Robo-Repulsive Cues Regulates Fibroblast Contact Inhibition of Locomotion. Dev. Cell *35*, 78–92. https://doi.org/10.1016/j.devcel.2015.09.002.

38. Remorino, A., De Beco, S., Cayrac, F., Di Federico, F., Cornilleau, G., Gautreau, A., Parrini, M.C., Masson, J.-B., Dahan, M., and Coppey, M. (2017). Gradients of Rac1 Nanoclusters Support Spatial Patterns of Rac1 Signaling. Cell Rep. *21*, 1922–1935. https://doi.org/10.1016/j.celrep.2017.10.069.

39. Das, S., Yin, T., Yang, Q., Zhang, J., Wu, Y.I., and Yu, J. (2015). Single-molecule tracking of small GTPase Rac1 uncovers spatial regulation of membrane translocation and mechanism for polarized signaling. Proc. Natl. Acad. Sci. USA *112*, E267–E276. https://doi.org/10.1073/pnas.1409667112.

40. Martin, K., Reimann, A., Fritz, R.D., Ryu, H., Jeon, N.L., and Pertz, O. (2016). Spatio-temporal co-ordination of RhoA, Rac1 and Cdc42 activation during prototypical edge protrusion and retraction dynamics. Sci. Rep. *6*, 21901. https://doi.org/10.1038/srep21901.

41. Levay, M., Krobert, K.A., Wittig, K., Voigt, N., Bermudez, M., Wolber, G., Dobrev, D., Levy, F.O., and Wieland, T. (2013). NSC23766, a Widely Used Inhibitor of Rac1 Activation, Additionally Acts as a Competitive Antagonist at Muscarinic Acetylcholine Receptors. J. Pharmacol. Exp. Therapeut. *347*, 69–79. https://doi.org/10.1124/jpet.113.207266.

42. Kai, Y., Motegi, M., Suzuki, Y., Harada, Y., Takeuchi, H., Kon, R., Ikarashi, N., Chiba, Y., Kamei, J., and Sakai, H. (2019). Increased Rac1 Activation in the Enhanced Carbachol-Induced Bronchial Smooth Muscle Contraction of Repeatedly Antigen-Challenged Mice. Biol. Pharm. Bull. *42*, 1605–1607. https://doi.org/10.1248/bpb.b19-00404.

43. Davis, M.J., Ha, B.H., Holman, E.C., Halaban, R., Schlessinger, J., and Boggon, T.J. (2013). RAC1^{P29S} is a spontaneously activating cancer-associated GTPase. Proc. Natl. Acad. Sci. USA *110*, 912–917. https://doi.org/10.1073/pnas.1220895110.

44. O'Loughlin, T., Masters, T.A., and Buss, F. (2018). The MYO6 interactome reveals adaptor complexes coordinating early endosome and cytoskeletal dynamics. EMBO Rep. *19*, e44884. https://doi.org/10.15252/embr.201744884.

45. Sobczak, M., Chumak, V., Pomorski, P., Wojtera, E., Majewski, Ł., Nowak, J., Yamauchi, J., and Rędowicz, M.J. (2016). Interaction of myosin VI and its binding partner DOCK7 plays an important role in NGF-stimulated protrusion formation in PC12 cells. Biochim. Biophys. Acta *1863*, 1589–1600. https://doi.org/10.1016/j.bbamcr.2016.03.020.

46. Kukimoto-Niino, M., Tsuda, K., Ihara, K., Mishima-Tsumagari, C., Honda, K., Ohsawa, N., and Shirouzu, M. (2019). Structural Basis for the Dual Substrate Specificity of DOCK7 Guanine Nucleotide Exchange Factor. Structure *27*, 741–748.e3. https://doi.org/10.1016/j.str.2019.02.001.

47. Majewski, Ł., Sobczak, M., Havrylov, S., Jóźwiak, J., and Rędowicz, M.J. (2012). Dock7: A GEF for Rho-family GTPases and a novel myosin VI-binding partner in neuronal PC12 cells. Biochem. Cell. Biol. *90*, 565–574. https://doi.org/10.1139/o2012-009.

48. He, F., Wollscheid, H.-P., Nowicka, U., Biancospino, M., Valentini, E., Ehlinger, A., Acconcia, F., Magistrati, E., Polo, S., and Walters, K.J. (2016). Myosin VI Contains a Compact Structural Motif that Binds to Ubiquitin Chains. Cell Rep. *14*, 2683–2694. https://doi.org/10.1016/j.celrep.2016.01.079.

49. Laurin, M., and Côté, J.F. (2014). Insights into the biological functions of Dock family guanine nucleotide exchange factors. Genes Dev. *28*, 533–547. https://doi.org/10.1101/gad.236349.113.

50. Côté, J.F., and Vuori, K. (2002). Identification of an evolutionarily conserved superfamily of DOCK180-related proteins with guanine nucleotide exchange activity. J. Cell Sci. *115*, 4901–4913. https://doi.org/10.1242/jcs.00219.

51. Kulkarni, K., Yang, J., Zhang, Z., and Barford, D. (2011). Multiple Factors Confer Specific Cdc42 and Rac Protein Activation by Dedicator of Cytokinesis (DOCK) Nucleotide Exchange Factors. Journal of Biological Chemistry *286*, 25341–25351. https://doi.org/10.1074/jbc.M111.236455.

52. Jumper, J., Evans, R., Pritzel, A., Green, T., Figurnov, M., Ronneberger, O., Tunyasuvunakool, K., Bates, R., Žídek, A., Potapenko, A., et al. (2021). Highly accurate protein structure prediction with AlphaFold. Nature *596*, 583–589. https://doi.org/10.1038/s41586-021-03819-2.

53. Tunyasuvunakool, K., Adler, J., Wu, Z., Green, T., Zielinski, M., Žídek, A., Bridgland, A., Cowie, A., Meyer, C., Laydon, A., et al. (2021). Highly accurate protein structure prediction for the human proteome. Nature *596*, 590–596. https://doi.org/10.1038/s41586-021-03828-1.

54. Cancer Genome Atlas Network (2012). Comprehensive molecular portraits of human breast tumours. Nature *490*, 61–70. https://doi.org/10.1038/nature11412.

55. Campanale, J.P., Mondo, J.A., and Montell, D.J. (2022). A Scribble/Cdep/Rac pathway controls follower-cell crawling and cluster cohesion during collective border-cell migration. Dev. Cell *57*, 2483–2496.e4. https://doi.org/10.1016/j.devcel.2022.10.004.

56. Vishwakarma, M., Di Russo, J., Probst, D., Schwarz, U.S., Das, T., and Spatz, J.P. (2018). Mechanical interactions among followers determine the emergence of leaders in migrating epithelial cell collectives. Nat. Commun. *9*, 3469. https://doi.org/10.1038/s41467-018-05927-6.

57. Biancospino, M., Buel, G.R., Niño, C.A., Maspero, E., Scotto di Perrotolo, R., Raimondi, A., Redlingshöfer, L., Weber, J., Brodsky, F.M., Walters, K.J., and Polo, S. (2019). Clathrin light chain A drives selective myosin VI recruitment to clathrin-coated pits under membrane tension. Nat. Commun. *10*, 4974. https://doi.org/10.1038/s41467-019-12855-6.

58. Magistrati, E., Maestrini, G., Niño, C.A., Lince-Faria, M., Beznoussenko, G., Mironov, A., Maspero, E., Bettencourt-Dias, M., and Polo, S. (2022).